energies

MDPI

Article

Electric Arc Furnaces as a Cause of Current and Voltage Asymmetry

Zbigniew Olczykowski

Faculty of Transport, Electrical Engineering and Computer Science, Kazimierz Pulaski University of Technology and Humanities, 26-600 Radom, Poland; z.olczykowski@uthrad.pl

Abstract: In the case of three-phase arc furnaces, two types of asymmetry can be distinguished: constructional and operational. The structural asymmetry is related to the construction of high-current circuits supplying the arc furnace. The knowledge of the parameters of the high-current circuit allows to determine the operating characteristics of the arc device. The author proposed a method for calculating the real values of the resistance and reactance of the high-current circuit. For this purpose, tests were made to short-circuit the electrodes with the charge. During the short-circuit, with the use of a power quality analyzer, measurements of electrical indicators were carried out, which allow to determine the parameters of the high-current circuit. A new method for determining voltage operational unbalance is also presented in this paper. The theoretical considerations presented in the article were verified in industrial conditions.

Keywords: current and voltage asymmetry; arc furnace; power quality; voltage fluctuations

check for updates

Citation: Olczykowski, Z. Electric Arc Furnaces as a Cause of Current and Voltage Asymmetry. *Energies* **2021**, *14*, 5058. https://doi.org/10.3390/en14165058

Academic Editor: José Matas

Received: 13 June 2021
Accepted: 13 August 2021
Published: 17 August 2021

Publisher's Note: MDPI stays neutral with regard to jurisdictional claims in published maps and institutional affiliations.

Copyright: © 2021 by the author. Licensee MDPI, Basel, Switzerland. This article is an open access article distributed under the terms and conditions of the Creative Commons Attribution (CC BY) license (https://creativecommons.org/licenses/by/4.0/).

1. Introduction

Voltage and current unbalance is one of the basic problems related to the power quality, which can cause many negative effects on the power system. For many years, the main causes of asymmetry were single-phase loads, which caused a different distribution of loads in individual phases. The voltage asymmetry also caused the asymmetry of the currents consumed by the symmetrical loads, which increased further asymmetry in the power supply system. The assessment of the increase in voltage unbalance in the PCC, which is the result of the interaction of many unbalanced loads, is presented in the publication [1]. The proposed method uses the voltages and currents consumed by individual consumers recorded in real conditions. The publication [2] presents the assessment of the influence of single-phase electric consumers on voltage asymmetry.

The attention was paid to disturbances caused by non-linear devices, including the influence on the value of the current in the neutral conductor. The need to monitor electrical power quality parameters was emphasized in order to set alarms to warn of exceeding the limit values.

Currently, in power systems, there are more and more distributed energy sources, mainly photovoltaic power plants. Photovoltaic installations affect the quality of the voltage on the supply line to which they are connected. They cause, among other things, an increase in voltage and voltage asymmetry. The assessment of the power quality of PV systems supplied from distribution grids was presented in the publications [3–6]. Also [7] presents an analysis of the impact of photovoltaic systems for power quality, including a voltage imbalance. Dynamic models of the single-phase PV units are developed and utilized. Other sources of voltage asymmetry that have emerged in recent years are charging stations for electric cars [8–10] and energy storage [11,12].

The increasing number of devices and installations disturbing the power quality forced the application of various remedial measures. An interesting method allowing to reduce the voltage and current asymmetry is presented in [13]. The applied strategy is particularly effective in smart grids and systems using electricity storage.

The concept of dynamic programming of inverters, aimed at limiting voltage asymmetry, has been presented in publications [14–16], and the use of STATCOM systems is presented in publications [17,18].

Current and voltage unbalance is also caused by three-phase receivers. The asymmetry is caused by the different load of the individual phases. We encounter a similar situation in the case of arc furnaces [19]. One of the reasons for the operational asymmetry are different values of currents in individual phases supplying the furnace transformer. As a result, there is a voltage asymmetry. Through the steelworks supply networks, the voltage asymmetry is propagated to the electrical system. Voltage asymmetry also causes disturbances in the operation of the arc furnace.

The operational asymmetry is reduced by the use of the electrode position control system [20,21] and additional devices aimed at improving the energy quality [22–25]. It should also be mentioned that the arc furnaces is the source of fast voltage fluctuations [26–31]. This electromagnetic disturbance occurs with the asymmetry of currents and voltages.

The article presents issues related to current and voltage asymmetry caused by arc furnaces. The publication is a continuation of the series of articles [32–34] presenting the impact of electric arc furnaces on the power system.

The article presents the methods of determining voltage asymmetry and relates them to the method proposed by the author (Section 4). Based on the analysis of power quality indicators measured in the supply lines of the steelworks, the constructional and operational asymmetry caused by arc furnaces was analyzed. The method for determining the parameters of the high-current path of the electric arc furnace is presented (Section 3).

The Discussion (Section 4) presents the values of the voltage unbalance coefficients K_{2U} determined by various methods and compared with the method proposed by the author—Table 1. Comments are presented in the Discussion and in the Conclusions.

Table 1. Values of the asymmetry coefficient calculated by various methods developed from [32].

Measured Voltages Expressed in Nominal Voltage (%)	K_{2U}							
	Measurement	IEC 61000-2-12	IEC 61000-4-30	IEC 61000-2-1 ANSI C84.1	GOST 13109-97	Nomogram I	Nomogram II	Author
105.85; 103.31; 104.68	1.45	1.402	1.401	1.247	1.3519	1.41	1.42	1.369
103.15; 101.41; 102.77	0.95	1.029	1.026	1.006	0.988	1.01	1.02	1.023
103.94; 101.73; 102.97	1.34	1.241	1.239	1.171	1.198	1.31	1.31	1.231
101.47; 101.36; 101.96	0.4	0.357	0.357	0.351	0.381	0.36	0.36	0.356

2. Methods of Determining Voltage Asymmetry

The method of symmetrical components can be classified as one of the most known methods of determining the asymmetry coefficient [35].

In the first symmetrical system (positive or direct sequence component U_{1L1}, U_{1L2}, U_{1L3}), the voltage phasors are shifted by an angle of 120° and has the same phase sequence as the asymmetrical voltage system U_{L1}, U_{L2}, U_{L3}; the second symmetrical system (negative or inverse sequence component U_{2L1}, U_{2L2}, U_{2L3}) has the reverse phase sequence; in the third symmetrical system (zero or homopolar sequence component U_{0L1}, U_{0L2}, U_{0L3}), the voltage phasors are in phase with each other:

- positive sequence

$$\begin{aligned} \underline{U}_{1L1} &= U_{1L1} = U_1 \\ \underline{U}_{1L2} &= a^2\underline{U}_{1L1} \\ \underline{U}_{1L3} &= a\underline{U}_{1L1} \end{aligned} \quad (1)$$

- negative sequence

$$\begin{aligned} \underline{U}_{2L1} &= \underline{U}_2 \\ \underline{U}_{2L2} &= a\underline{U}_{2L1} \\ \underline{U}_{2L3} &= a^2\underline{U}_{2L1} \end{aligned} \quad (2)$$

- zero sequence

$$\underline{U}_{0L1} = \underline{U}_{0L2} = \underline{U}_{0L3} = \underline{U}_0 \tag{3}$$

where a is the operator of rotation:

The phase voltages are the sum of the symmetrical components:

$$\begin{array}{c} a = e^{j\frac{2}{3}\pi} = -\frac{1}{2} + j\frac{\sqrt{3}}{2} \\ a^2 = e^{j\frac{4}{3}\pi} = e^{-j\frac{2}{3}\pi} = -\frac{1}{2} - j\frac{\sqrt{3}}{2} \end{array} \tag{4}$$

$$\begin{array}{c} \underline{U}_{L1} = \underline{U}_{1L1} + \underline{U}_{2L1} + \underline{U}_{0L1} \\ \underline{U}_{L2} = \underline{U}_{1L2} + \underline{U}_{2L2} + \underline{U}_{0L2} = a^2\underline{U}_{1L1} + a\underline{U}_{2L1} + \underline{U}_{0L1} \\ \underline{U}_{L3} = \underline{U}_{1L3} + \underline{U}_{2L3} + \underline{U}_{0L3} = a\underline{U}_{1L1} + a^2\underline{U}_{2L1} + \underline{U}_{0L1} \end{array} \tag{5}$$

The phase-to-phase voltages as a function of symmetrical components can be presented as the difference of the respective phase voltages:

$$\begin{array}{l} \underline{U}_{L12} = \underline{U}_{L1} - \underline{U}_{L2} = (1 - a^2)\underline{U}_{1L1} + (1 - a)\underline{U}_{2L1} \\ \underline{U}_{L23} = \underline{U}_{L2} - \underline{U}_{L3} = (a^2 - a)\underline{U}_{1L1} + (a - a^2)\underline{U}_{2L1} \\ \underline{U}_{L31} = \underline{U}_{L3} - \underline{U}_{L1} = (a - 1)\underline{U}_{1L1} + (a^2 - 1)\underline{U}_{2L1} \end{array} \tag{6}$$

The complex factor $\underline{K}_{2U}$ is:

$$\underline{K}_{2U} = \frac{\underline{U}_2}{\underline{U}_1} = \frac{\underline{U}_{L1} + a^2 \cdot \underline{U}_{L2} + a \cdot \underline{U}_{L3}}{\underline{U}_{L1} + a \cdot \underline{U}_{L2} + a^2 \cdot \underline{U}_{L3}} = \frac{U_2}{U_1} \cdot e^{j\Psi_u} \tag{7}$$

Ignoring the phase shift angle between the positive and negative components, we get:

$$|\underline{K}_{2U}| = \frac{|\underline{U}_{L1} + a^2 \cdot \underline{U}_{L2} + a \cdot \underline{U}_{L3}|}{|\underline{U}_{L1} + a \cdot \underline{U}_{L2} + a^2 \cdot \underline{U}_{L3}|} = \frac{U_2}{U_1} \tag{8}$$

To assess the voltage asymmetry level, the most common is the asymmetry coefficient expressed in percent, which is the ratio the negative to the positive sequence:

$$K_{2U} = \frac{U_2}{U_1} 100\% \tag{9}$$

According to the EN 61000-4-30 [36] standard, the value of the K_{2U} asymmetry coefficient is determined by the relationship:

$$K_{2U} = \sqrt{\frac{1 - \sqrt{3 - 6 \cdot \beta}}{1 + \sqrt{3 - 6 \cdot \beta}}} 100\% \tag{10}$$

where β:

$$\beta = \frac{U_{L12}^4 + U_{L23}^4 + U_{L31}^4}{\left(U_{L12}^2 + U_{L23}^2 + U_{L31}^2\right)^2} \tag{11}$$

and according to the norm IEC 61000-2-12 [37] formula:

$$K_{2U} = \sqrt{\frac{6(U_{L12}^2 + U_{L23}^2 + U_{L31}^2)}{\left(U_{L12} + U_{L23} + U_{L31}\right)^2} - 2} \tag{12}$$

and by IEC 61000-2-1 [38], ANSI C84.1 [39], P29 [40] formula:

$$K_{2U} = \frac{\Delta U_{max}}{U_{ave}} 100\% \tag{13}$$

where:

ΔU_{max}—maximum phase voltage deviation from the average value of three phase voltages

U_{ave}—average value of three phase voltages.

In GOST 13109-97 the asymmetry coefficient K_{2U} determined from the formulas [41]:

$$K_{2U} = \frac{\sqrt{\frac{1}{12}\left(\left[\left(\sqrt{3}U_{L12} - \sqrt{4U_{L23}^2 - \left(\frac{U_{L23}^2 - U_{L31}^2}{U_{L12}} + U_{L12}\right)^2}\right)^2 + \left(\frac{U_{L23}^2 - U_{L31}^2}{U_{L12}}\right)^2\right]\right.}}{\sqrt{\frac{1}{12}\left(\left[\left(\sqrt{3}U_{L12} + \sqrt{4U_{L23}^2 - \left(\frac{U_{L23}^2 - U_{L31}^2}{U_{L12}} + U_{L12}\right)^2}\right)^2 + \left(\frac{U_{L23}^2 - U_{L31}^2}{U_{L12}}\right)^2\right]\right.}} 100\% \quad (14)$$

where:

$$U_1 = \sqrt{\frac{1}{12}\left(\left[\left(\sqrt{3}U_{L12} + \sqrt{4U_{L23}^2 - \left(\frac{U_{L23}^2 - U_{L31}^2}{U_{L12}} + U_{L12}\right)^2}\right)^2 + \left(\frac{U_{L23}^2 - U_{L31}^2}{U_{L12}}\right)^2\right]\right.} \quad (15)$$

$$U_2 = \sqrt{\frac{1}{12}\left(\left[\left(\sqrt{3}U_{L12} - \sqrt{4U_{L23}^2 - \left(\frac{U_{L23}^2 - U_{L31}^2}{U_{L12}} + U_{L12}\right)^2}\right)^2 + \left(\frac{U_{L23}^2 - U_{L31}^2}{U_{L12}}\right)^2\right]\right.} \quad (16)$$

Using the Kowzan method based on nomographs, described in [42], the asymmetry coefficient is determined from the formula (17):

$$\frac{A_C}{A_A} = \frac{U_{L31}}{U_{L12}}; \frac{A_B}{A_A} = \frac{U_{L23}}{U_{L12}} \quad (17)$$

then K_{2U} is read from the nomogram.

Another method using nomographs was developed at the Institute of Energy of Ukraine [42]. The asymmetry coefficient K_{2U} was determined according to the dependence (18).

$$x = \frac{U_{L12}}{U_{L31}}; y = \frac{U_{L21}}{U_{L31}} \quad (18)$$

As in the previous method, K_{2U} is read from the nomogram. Examples of nomograms are presented in the publication [42].

The article presents a new method for determining voltage asymmetry. Knowing the voltage modules U_{L12}, U_{L23}, U_{L31}, the squares of the modules can be determined U_{L12}^2, U_{L23}^2, U_{L31}^2.

$$U_{L12}^2 = U_M^2 + W_{U^2} \cdot \cos \alpha_{U^2} \quad (19)$$

$$U_{L32}^2 = U_M^2 + W_{U^2} \cos(\alpha_{U^2} - 120^o) \quad (20)$$

$$U_{L31}^2 = U_M^2 + W_{U^2} \cdot \cos(\alpha_{U^2} + 120^o) \quad (21)$$

For the voltages U_{L12}, U_{L23}, U_{L31}, the mean value of the squares of the voltages was calculated U_M^2:

$$U_M^2 = \frac{U_{L12}^2 + U_{L23}^2 + U_{L31}^2}{3} \quad (22)$$

$$W_{U^2} \cdot \cos \alpha_{U^2} = U_{L12}^2 - U_M^2 \quad (23)$$

$$W_{U^2} \cdot \sin \alpha_{U^2} = \frac{1}{\sqrt{3}}(U_{L23}^2 - U_{L31}^2) \quad (24)$$

and a differential module W_{U^2} asymmetry, in the form of:

$$W_{U^2} = \frac{\sqrt{2}}{3}\sqrt{\left(U_{L12}^2 - U_{L23}^2\right)^2 + \left(U_{L23}^2 - U_{L31}^2\right)^2 + \left(U_{L31}^2 - U_{L12}^2\right)^2} \quad (25)$$

$$\alpha_{U^2} = \text{arctg}\frac{U_{L23}^2 - U_{L31}^2}{\sqrt{3}(2U_{L12}^2 - U_{L23}^2 - U_{L31}^2)} + \left[1 - \text{sign}(2U_{L12}^2 - U_{L23}^2 - U_{L31}^2)\right]\cdot 90^o \quad (26)$$

To evaluate the asymmetry of the voltage squares, the difference-angle factor of the asymmetry would be used:

$$\underline{k}_{U^2} = k_{U^2}e^{j\alpha_{U^2}} \quad (27)$$

Then, the asymmetry differential coefficient was determined k_{U^2}

$$k_{U^2} = \frac{W_{U^2}}{U_M^2} = \sqrt{2}\frac{\sqrt{\left(U_{L12}^2 - U_{L23}^2\right)^2 + \left(U_{L23}^2 - U_{L31}^2\right)^2 + \left(U_{L31}^2 - U_{L32}^2\right)^2}}{\left(U_{L12}^2 + U_{L23}^2 + U_{L31}^2\right)} \quad (28)$$

It is found that $3 - 6\cdot\beta = 1 - k_{U^2}^2$. Consequently, the voltage asymmetry factor will be:

$$K_{2U} = \sqrt{\frac{1-\sqrt{1-k_{U^2}^2}}{1+\sqrt{1-k_{U^2}^2}}} = \sqrt{\frac{\left(1-\sqrt{1-k_{U^2}^2}\right)^2}{\left(1-\sqrt{1-k_{U^2}^2}\right)\left(1+\sqrt{1-k_{U^2}^2}\right)}} = \frac{1-\sqrt{1-k_{U^2}^2}}{\sqrt{1-\left(1-k_{U^2}^2\right)}} = \frac{1-\sqrt{1-k_{U^2}^2}}{k_{U^2}^2} \quad (29)$$

In the case of a small value of voltage unbalance, the K_{2U} coefficient can be described by the Equation (29):

$$K_{2U} \approx 0.5k_{U^2} \quad (30)$$

3. Asymmetry Caused by Arc Furnaces

In the case of three-phase arc furnaces, two types of asymmetry can be distinguished: constructional and operational.

3.1. Constructional Asymmetry

As a result of different impedance values of the individual phases in the high-current path of the electric arc furnace, a constructional asymmetry arises. Knowledge of the parameters of the high-current circuit allows for the determination of the operating characteristics of the arc furnace and is necessary to determine the settings of the electrode position regulator.

Figure 1 shows the measurement system with the connection point for power quality analyzers. During the recording of electrical parameters (currents, voltages, power), the electrodes were shorted several times with the charge of the arc furnace. The method of determining the parameters of the high-current path, based on the data obtained during measurements with the use of power quality analyzers, has been patented and verified in real conditions [43].

After the electrodes are immersed in the molten metal, they are immobilized. During this time, complete short circuit of the electric arc supply system in the electric arc furnace.

Figure 2 shows the changes in active and reactive power recorded during smelting, when the electrodes were short-circuit with the charge, and Figure 3 shows a circle diagram for the furnace during the short-circuit test. Records of currents, voltages and power (necessary to determine the reactance and resistance of the high-current circuit) were made using a 3-phase power quality analyzer-Memobox 800—Figure 1. Figure 4 shows the changes in voltage and current recorded in one of the phases on the primary side of the furnace transformer (supply line to the steel plant) during the short-circuit test.

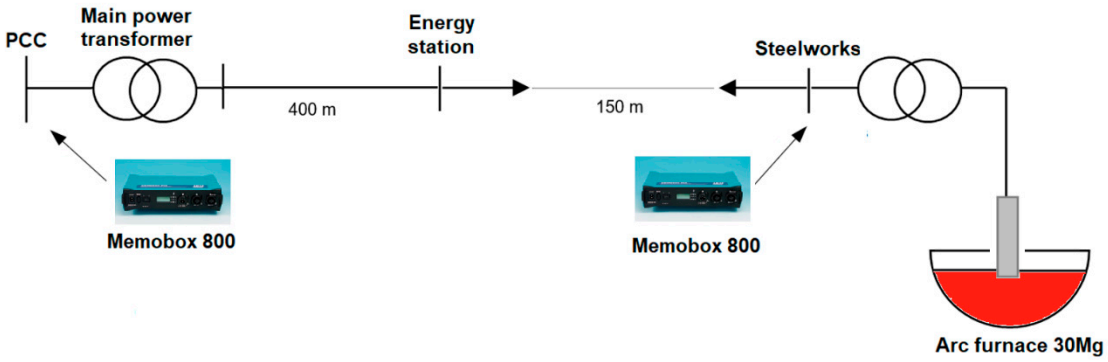

Figure 1. Place of measurement of electrical parameters.

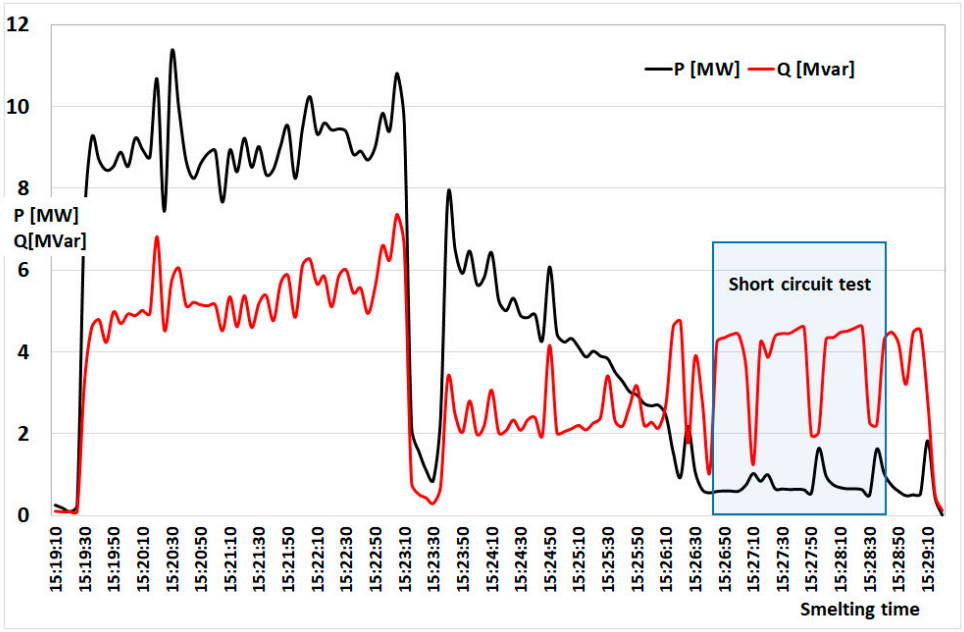

Figure 2. Changes in active and reactive power during smelting when the electrodes were short-circuited with the charge.

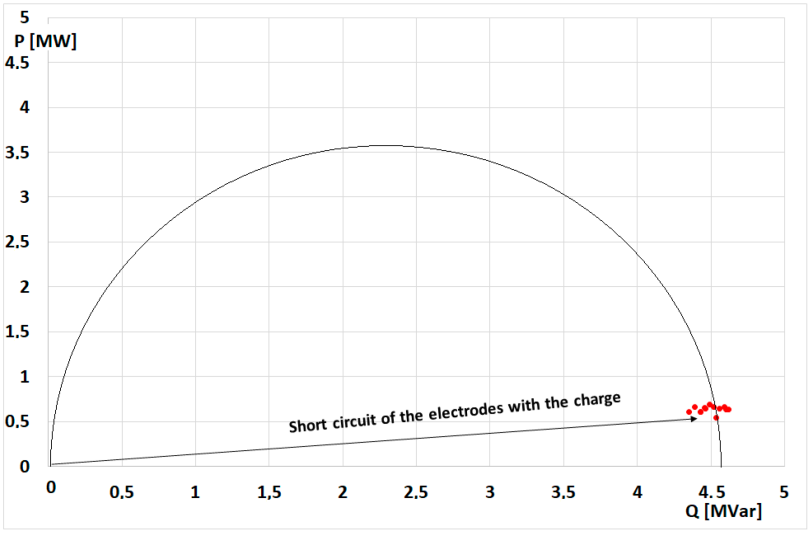

Figure 3. Circle diagram of an arc furnace for the short-circuit condition of the electrodes to the charge.

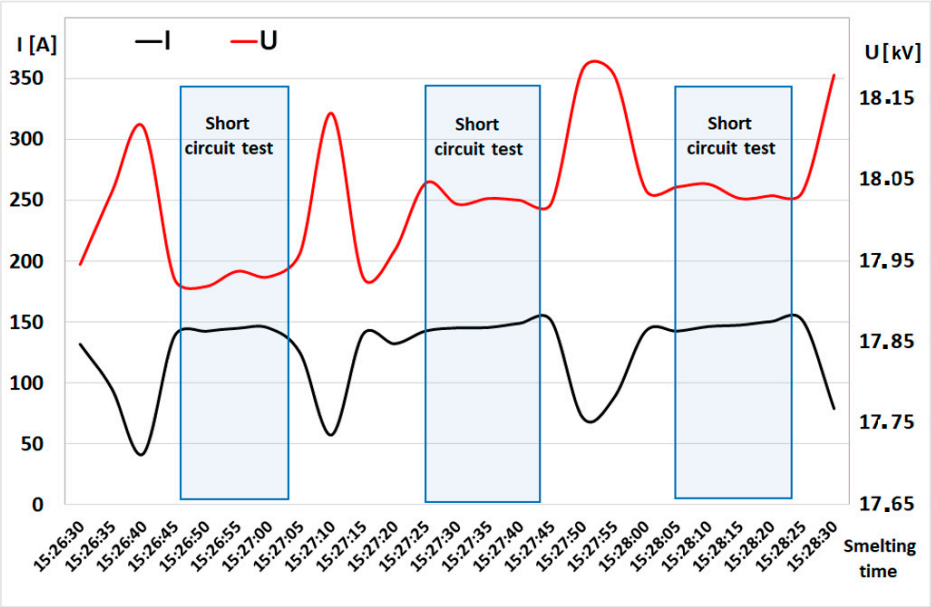

Figure 4. Voltage and current changes during the test of short-circuit of the electrodes with the charge.

The following part of the article presents an example of determining the impedance of a high-current circuit on the basis of measurements of power, voltage and current when the electrodes are short-circuited with the charge. The calculations, as an example, show the determination of high-current path parameters for one phase.

The impedance is calculated from the formula:

$$Z_1 = \frac{U_{L1}}{I_{L1}} \tag{31}$$

and the resistance from the formula:

$$R_1 = \frac{P_1}{I_{L1}^2} \tag{32}$$

The reactance can be determined from formula:

$$X_1 = \sqrt{Z_1^2 - R_1^2} \tag{33}$$

The transformer parameters are based on its rated data. In the calculations, they were related to the primary side, and then the final calculations were converted to the secondary side.

The transformer impedance is:

$$Z_T = \frac{\Delta U_{SCV} \cdot U_n^2}{100 \cdot S_n} \tag{34}$$

resistance is as follows:

$$R_T = \frac{\Delta P_{Cu} \cdot U_n^2}{S_n^2} \tag{35}$$

and transformer reactance:

$$X_T = \sqrt{Z_T^2 - R_T^2} \tag{36}$$

The resistance and reactance of the high-current circuit related to the upper voltage are as follows:

$$R_{hct} = R_1 - R_T \tag{37}$$

$$X_{hct} = X_1 - X_T \tag{38}$$

After converting to the secondary side at the k_T ratio, we get the values of resistance and reactance of the high-current path (without reactance and resistance of the transformer):

$$R_{2hct} = \frac{R_{hct}}{k_T^2} \tag{39}$$

$$X_{2hct} = \frac{X_{hct}}{k_T^2} \tag{40}$$

where:

S_n—rated apparent power (MVA);
k_T—ratio of the nominal voltage U_{1H} of the upper voltage winding to the rated voltage U_{1L} of the lower voltage winding;
ΔP_{Cu}—rated active power losses in transformer windings (MW);
ΔU_{scv}—short-circuit voltage as a percentage of the rated voltage (%).

The further part of the article presents the calculations of the high-current path parameters for an exemplary furnace installation, the supply diagram of which is shown in Figure 1.

Calculations of the resistance and reactance of the high-current track with the furnace transformer related to the primary side of U_{L1} are as follows:

$$Z_1 = \frac{U_{L1}}{I_{L1}} = \frac{18411.7V}{145.2A} = 126.80\Omega \tag{41}$$

$$R_1 = \frac{P_1}{I_{L1}^2} = \frac{0.635MW}{(145.2\ A)^2} = 30.11\Omega \tag{42}$$

$$X_1 = \sqrt{Z_1^2 - R_1^2} = \sqrt{126.8^2 - 26.09^2} = 123.17\Omega \tag{43}$$

The rated data of the furnace transformer are as follows:

S_n—rated apparent power (MVA); S_n = 10.606 MVA;
k_T—ratio of the nominal voltage U_{1H} of the upper voltage winding to the nominal voltage U_{1L} of the lower voltage winding; k_T = 200
ΔP_{Cu}—nominal active power losses in transformer windings (MW); ΔP_{Cu} = 0.179885 MW
ΔU_{scv}—short-circuit voltage as a percentage of the rated voltage (%). ΔU_{scv} = 14.91%

The transformer impedance is:

$$Z_T = \frac{\Delta U_{scv} \cdot U_n^2}{100 \cdot S_n} = \frac{14.91 \cdot (30kV)^2}{100 \cdot 10.606VA} = 12.65\Omega \tag{44}$$

resistance is as follows:

$$R_T = \frac{\Delta P_{Cu} \cdot U_n}{S_n^2} = \frac{0.179885MW \cdot (30kV)^2}{(10.606\ MVA)^2} = 1.44\Omega \tag{45}$$

and transformer reactance:

$$X_T = \sqrt{Z_T^2 - R_T^2} = \sqrt{12.65^2 - 1.44^2} = 12.57\Omega \tag{46}$$

The resistance and reactance of the high-current circuit related to the upper voltage are:

$$R_{hct} = R_1 - R_T = 30.11 - 1.44 = 28.67\Omega \tag{47}$$

$$X_{hct} = X_1 - X_T = 123.17 - 12.57 = 110.6\Omega \tag{48}$$

After conversion to the secondary side at the ratio k_T = 200, the values of resistance and reactance of the high-current track (without reactance and resistance of the transformer) are:

$$R_{2hct} = \frac{R_{hct}}{k_T^2} = \frac{28.67\Omega}{200^2} = 0.717m\Omega \quad (49)$$

$$X_{2hct} = \frac{X_{hct}}{k_T^2} = \frac{110.6\Omega}{200^2} = 2.76m\Omega \quad (50)$$

For comparison, alternative calculations of the parameters of the high-current path proposed in the standard are presented [44].

The calculations of the high-current track reactance were made without taking into account the resistances, which in furnace devices do not have a significant impact on the short-circuit currents.

The short-circuit power of the network at the connection point of the furnace transformer is S_{SC} = 500 MVA.

The parameters of the furnace transformer on the "+", "0" and "−" taps are as follows:

S_n—rated apparent power: 20/20 − 15.935 − 8.314 MVA,
I_n—nominal currents:0.3849 − 0.3067 − 0.16/27.169 − 32.00 − 32.00 kA,
k_T—nominal ratio of transformer:30 kV/425 − 287.5 − 150 V,
ΔU_{scv}—short-circuit voltage as a percentage of the nominal voltage: 5.33 − 8.99 − 20.66%.

The multiplicity of the set short-circuit current of the transformer supplying the arc furnace i_{sc} is expressed by the relationship:

$$i_{sc} = \frac{100}{x_{hct} + x_{scv} + x_s} \quad (51)$$

where:

x_{hct}—reactance in (%) of high-current path of arc furnace,
x_{scv}—transformer short-circuit reactance (equal to short-circuit voltage) in (%),
x_s—network reactance in (%) "seen" from the transformer terminals.

The short-circuit loop reactance presented (excluding the transformer itself, for which they are set values) determine the dependencies:

$$x_{hc} = \frac{I_{LV} \cdot X_{hct}}{U_{LV}} \cdot 100\% \quad (52)$$

where:

I_{LV}—nominal phase current of the LV side of the transformer corresponding to the given tap,
X_{hcv}—high-current circuit reactance,
U_{LV}—nominal voltage of the given tap on the LV side of the transformer.

HV network reactance:

$$x_s = \frac{S_n}{S_{sc}} \cdot 100\% \quad (53)$$

where:

S_n—transformer rated apparent power at a given tap in (MVA),
S_{sc}—short-circuit apparent power of the network in (MVA).

In the case under consideration, the short-circuit current factor i_{scf} = 1.133, corresponding to the ratio of the current measured during the transformer short-circuit test and the transformer's rated current corresponding to a given tap, was assumed for calculations.

$$i_{scf} = \frac{201.22A}{204A} = 0.9863 \quad (54)$$

$$x_{sct} = u_{\%} = 15.09\% \quad (55)$$

$$x_s = \frac{10.606\text{MVA}}{500\text{MVA}} \cdot 100\% = 2.12\% \quad (56)$$

$$i_{scf} = \frac{100}{x_{hct} + x_{sct} + x_s} \quad (57)$$

$$x_{hct} = \frac{100 - i_{scf} \cdot (x_{sct} + x_s)}{i_{scf}} \quad (58)$$

$$x_{hct} = \frac{100 - 0.9863 \cdot (15.09 + 2.12)}{0.9863} = 84.18\% \quad (59)$$

$$x_{hct} = \frac{I_{LV} \cdot x_{hct}}{U_{LV}} \cdot 100\% \quad (60)$$

Taking account the expression in relative result the high-current circuit reactance:

$$X_{hct} = \frac{x_{hct} \cdot U_{LV}}{I_{LV} \cdot 100\%} = \frac{84.18\% \cdot 110.45\text{V}}{32.0\text{kA} \cdot 100\%} = 2.905\text{m}\Omega \quad (61)$$

3.2. Operational Asymmetry

Operational asymmetry results from the change in arc resistance caused by a different arc length during the smelting process.

Due to various changes in the parameters of the electric arc in the individual stages of the smelting, the currents flowing in the supply line of the arc furnace also change. The effect of current asymmetry is the voltage asymmetry, which may affect the correct operation of other devices.

The value of the unbalance factor K_{2U} is largely influenced by the relationship between the short-circuit power of the supply network and the furnace transformer power. This dependence can be written by the formula:

$$K_{2U} = K_{2I} \frac{1.1 S_n}{S_{sc}} \quad (62)$$

where:

K_{2U}—voltage asymmetry factor
K_{2I}—current asymmetry factor
S_n—rated apparent power of arc furnace transformer
S_{sc}—short-circuit apparent power of the supply network

Based on the measurements carried out in the supply networks of the arc furnaces, it was found that the current asymmetry coefficient rarely exceeds the value of 30% [45].

Assuming according to [46,47] $K_{2U} \leq 1\%$ for lines with voltage above 110 kV and $K_{2U} \leq 2\%$ for lines up to 110 kV, it is possible to define the conditions under which unacceptable voltage asymmetry will not occur.

For lines with a voltage of 110 kV and above:

$$0.3 \frac{1.1 S_n}{S_{SC}} \leq 0.01 \quad (63)$$

which corresponds to:

$$\frac{S_n}{S_{SC}} \leq 0.03 \quad (64)$$

For lines with a voltage of up to 1kV:

$$0.3 \frac{1.1 S_n}{S_{SC}} \leq 0.02 \quad (65)$$

which corresponds to:

$$\frac{S_n}{S_{SC}} \leq 0.06 \tag{66}$$

The changes in the voltage unbalance factor K_{2U} recorded in the weekly measurement cycle are shown in Figure 5. Measurements were made in the supply line to the steelworks (110 kV) and in the supply line for the furnace transformer (30 kV).

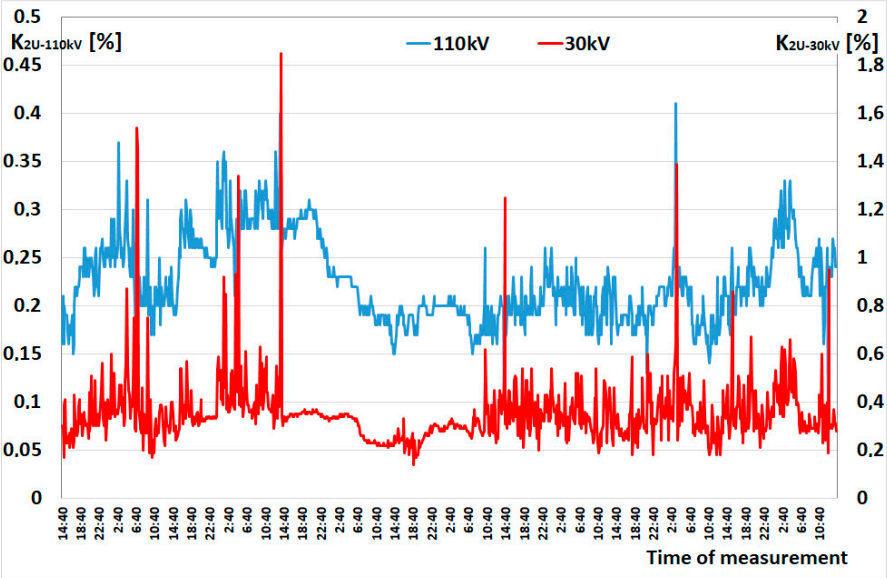

Figure 5. Changes in the asymmetry coefficient recorded during the weekly measurement cycle in the supply lines of the steel plant (110 kV) and the furnace transformer (30 kV).

The short-circuit apparent power of the network in relation to the rated apparent power of the furnace transformer at the measurement points is so high that the arc furnace does not significantly affect the voltage asymmetry. The momentary increase in the voltage unbalance factor at the level of medium voltage (30 kV) is the result of disturbances caused by the arc furnace in the initial stage of smelting.

According to formula (63), the short-circuit apparent power of the supply network should be about 33 times greater than the rated apparent power of the furnace transformer, so that the voltage unbalance factor does not exceed 1%.

Figure 6 shows the changes in the currents and the asymmetry coefficient (average values measured over a measuring interval of five seconds) recorded in the steel plant supply network during one smelting.

In the initial stage of smelting, the values of the currents are the highest and differ in particular phases. Before the ignition of the electric arc, there are moments of short-circuit of individual electrodes with the charge, and these may be short-circuits of one, two or three electrodes. At this time, the asymmetry factor reaches its greatest values. Along with the melting of the charge, when the currents flow more and more steadily, the voltage asymmetry decreases.

The structural and operational asymmetry caused by the operation of the arc furnace leads to: asymmetric distribution of heating powers emitted in the electric arcs in individual phases, uneven thermal load on the internal walls of the furnace and faster wear of the electrodes in the phase in which the highest current flows. The purpose of the electric arc regulators (electrode position regulators) is to symmetrize the power dissipated in the arcs of individual phases, therefore they do not reduce the current asymmetry.

The method presented in the article, based on the data recorded during the short-circuit test of the electrodes with the charge, allows to calculate the actual parameters of the

high-current circuit. Knowing the values of the high-current circuit parameters is helpful in determining the settings of the electrode adjuster.

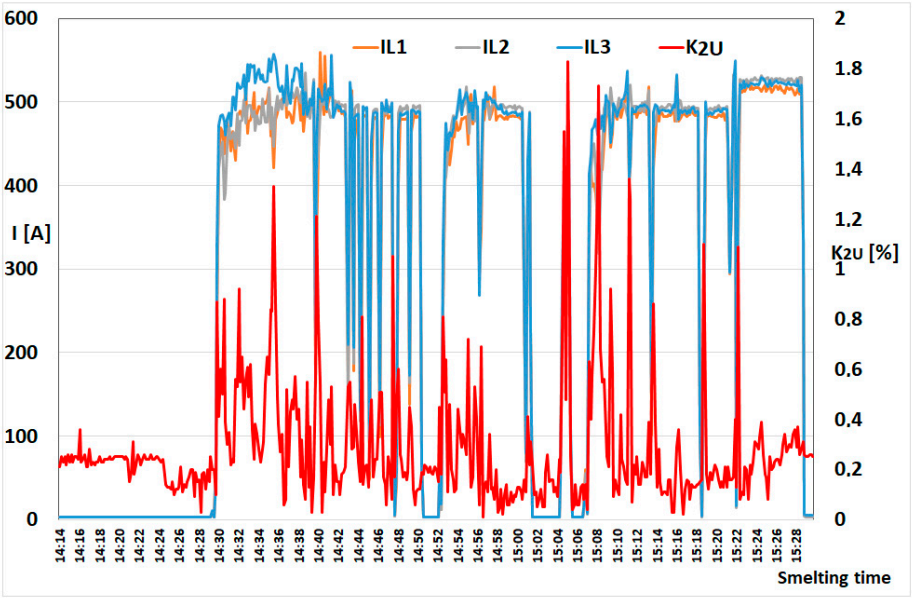

Figure 6. Changes in the currents in individual phases and the asymmetry coefficient recorded in the steel plant supply network during one smelting.

4. Discussion

4.1. Comparison of the Asymmetry Coefficient Determined by Various Methods

The voltage asymmetry in the supply line of arc furnaces can be determined in two ways: based on the analysis of the measurement results of the asymmetry index or calculated based on known voltage values. Assessing the asymmetry on the basis of data recorded with the use of energy quality indicators seems to be the best method of assessing the K_{2U} coefficient, because the voltage and current asymmetry value changes during the smelting process. The proposed method of determining the asymmetry factor K_{2U}, Formulas (29) and (30), allows to determine the voltage asymmetry on the basis of known voltage values.

Table 1 shows the values of the voltage unbalance coefficients K_{2U} determined by various methods and measured in the steel plant supply network.

The method of differential coefficients proposed by the author allows for the determination of the asymmetry coefficient with an average error, in relation to the reference values, averaging 0.87%, which is close to the error in the method presented in GOST 13109-97 [41] 0.94%.

Table 2 presents the values of the voltage asymmetry coefficients K_{2U} proposed in [42] and determined by various methods, including the method proposed by the author.

Table 2. Values of the asymmetry coefficient calculated by various methods and developed from data from [42].

Voltages (%) According to Data from [42]	K_{2U}							
	Calculation	IEC 61000-2-12	IEC 61000-4-30	IEC 61000-2-1 ANSI C84.1	GOST 13109-97	Nomogram I	Nomogram II	Author
94.54; 103.18; 89.55	8.6	8.318	8.427	7.53	8.437	8.62	8.61	8.343
102.67; 109.33; 96.00	7.6	7.498	7.521	6.491	7.522	7.55	7.51	7.456

4.2. Power Asymmetry

When using arc furnaces, the aim is to evenly distribute the power in the electric arcs of individual phases (active powers). Figure 7 shows the changes in active power

registered during one melting in the arc furnace. The mean values of active powers were determined in ten seconds measuring intervals.

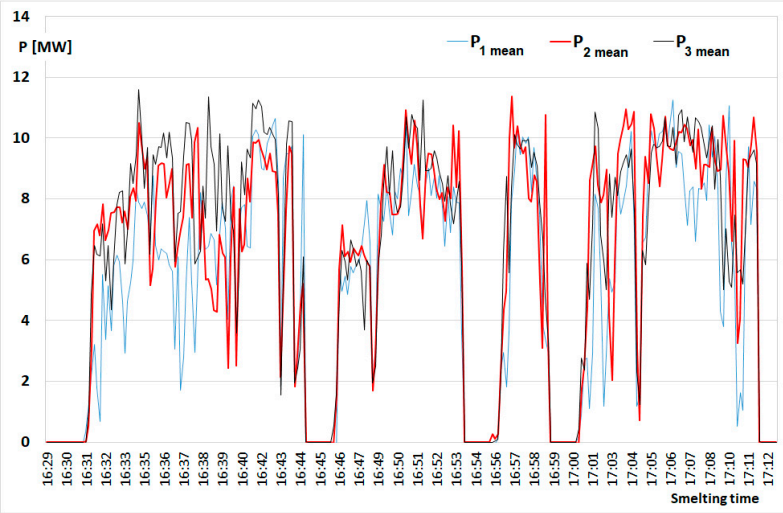

Figure 7. Changes in active power recorded during one melting in the arc furnace.

The correlation coefficients between the active power recorded in individual phases are as follows:

$$r_{P_1P_2} = 0.862;\ r_{P_1P_3} = 0.890;\ r_{P_2P_3} = 0.906 \quad (67)$$

Figure 8 shows correlation between the active power recorded in phase L_1 and phase L_2.

The electrode position controller is responsible for maintaining the symmetry of the heating power (the power generated in the electric arcs). The electrode position control system is characterized by a certain inertia. In the initial phase of melting the scrap, the electric arc is unstable. The currents in individual phases change dynamically, causing operational voltage asymmetry. The electrode position controller is not able to react quickly to changes in electric arc voltage. As a result, there are equally large changes in active power. Figure 9 shows the changes in the average, maximum and minimum power recorded during the smelting of steel in the arc furnace (for ten seconds measuring intervals).

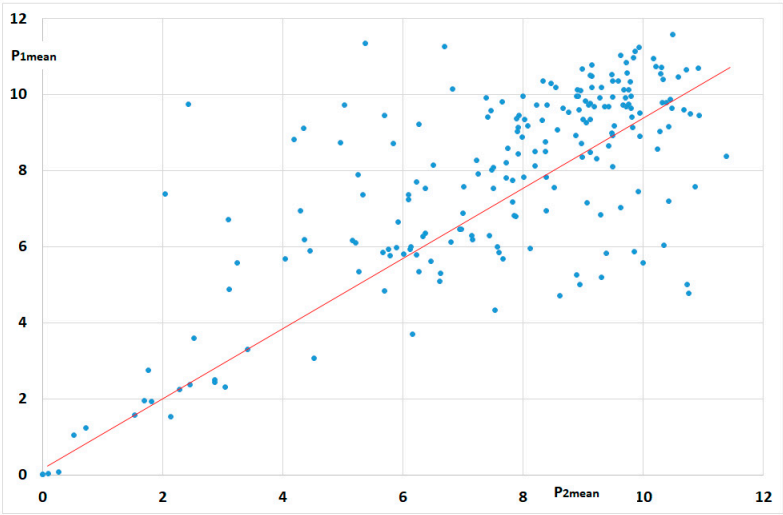

Figure 8. Correlation between the active power recorded in phase L_1 and phase L_2.

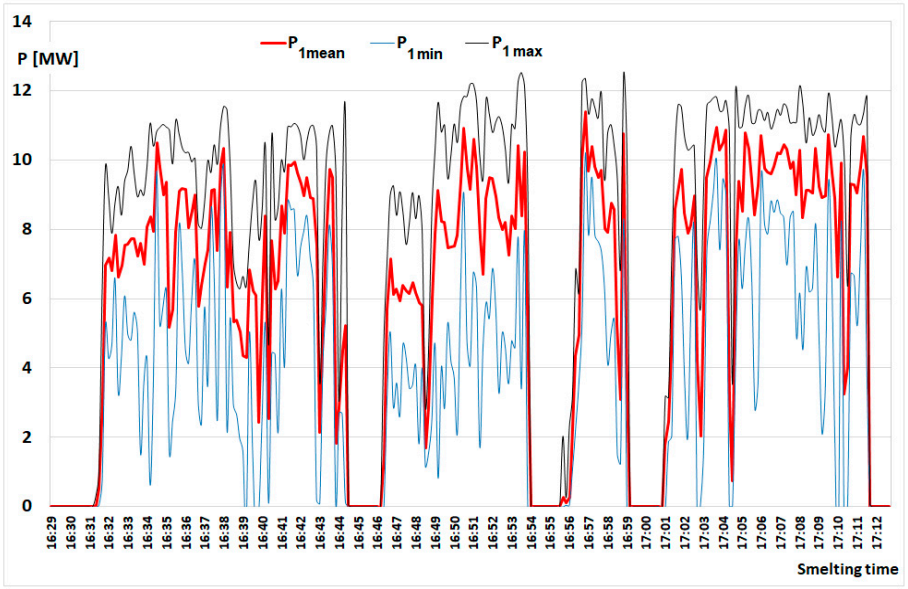

Figure 9. Changes in active power recorded in phase L_1 during one melting in the arc furnace.

Based on the analysis of measurement data, it can be concluded that the size of voltage unbalance is decisively influenced by the short-circuit power of the network in relation to the power of arc devices. Especially in the initial stage of the smelting, when the electric arc is initiated, rapid changes in the asymmetry coefficient were registered.

4.3. Author's Contribution

The author's task was to develop methods to estimate the asymmetry caused by arc furnaces:

- Contribution to the theoretical issues related to the operation of arc furnaces is the proposed method for determining the voltage asymmetry coefficient based on differential module and differential angle—Formulas (25) and (26).
- The calculated voltage unbalance factors K_{2U} using the method proposed by the author were compared with the values of K_{2U} determined by other methods, Tables 1 and 2.
- The proposed method for determining the parameters of the high-current circuit (structural asymmetry of the high-current circuit) based on measurements of electrical quantities in the network supplying arc furnaces has been verified in industrial conditions and has been patented.
- The waveforms of power quality parameters presented in the article were recorded by the author during several dozen measurement cycles in the networks supplying arc furnaces. This contributes to the expansion of practical knowledge about the impact of electric arc furnaces on the power system.

5. Conclusions

The method has been patented and verified in real conditions. The operational asymmetry is limited thanks to the electrode position control system. For the efficient operation of this system, it is necessary to know the actual parameters of the high-current circuit. The method of their determination developed by the author is based on data obtained from analyzers of electric energy quality parameters when the electrodes are short-circuited with the charge. The high-current circuit reactance determined by the author, in relation to the reactance determined by the electrode supplier, differs by approx. 1%, and in relation to the one calculated according to the standard [44] by 4.12%, where the high-current circuit resistance is neglected.

In the further part of the research on the asymmetry caused by arc furnaces, the author plans to determine the effect of compensating devices on reducing the asymmetry coefficient.

Funding: This research received no external funding.

Conflicts of Interest: The author declares no conflict of interest.

References

1. Sun, Y.; Li, P.; Li, S.; Zhang, L. Contribution determination for multiple unbalanced sources at the point of common coupling. *Energies* **2017**, *10*, 171. [CrossRef]
2. Popa, G.N.; Iagăr, A.; Diniș, C.M. Considerations on current and voltage unbalance of nonlinear loads in residential and educational sectors. *Energies* **2021**, *14*, 102. [CrossRef]
3. Al-Shetwi, A.Q.; Hannan, M.A.; Jern, K.P.; Alkahtani, A.A.; PG Abas, A.E. Power quality assessment of grid-connected PV system in compliance with the recent integration requirements. *Electronics* **2020**, *9*, 366. [CrossRef]
4. Antić, T.; Capuder, T.; Bolfek, M. A Comprehensive analysis of the voltage unbalance factor in pv and ev rich non-synthetic low voltage distribution networks. *Energies* **2021**, *14*, 117. [CrossRef]
5. Püvi, V.; Lehtonen, M. Convex Model for estimation of single-phase photovoltaic impact on existing voltage unbalance in distribution networks. *Appl. Sci.* **2020**, *10*, 8884. [CrossRef]
6. Lin, S.; He, S.; Zhang, H.; Liu, M.; Tang, Z.; Jiang, H.; Song, Y. Robust optimal allocation of decentralized reactive power compensation in three-phase four-wire low-voltage distribution networks considering the uncertainty. *Energies* **2019**, *12*, 2479. [CrossRef]
7. Islam, M.; Mithulananthan, N.; Hossain, J.; Shah, R. Dynamic voltage stability of unbalanced distribution system with high penetration of single-phase PV units. *J. Eng.* **2019**, *2019*, 4074–4080. [CrossRef]
8. Roy, R.B.; Alahakoon, A.; Arachchillage, S.J. Grid impacts of uncoordinated fast charging of electric ferry. *Batteries* **2021**, *7*, 13. [CrossRef]
9. Rodríguez-Pajarón, P.; Hernández, A.; Jovica, V.; Milanović, J.V. Probabilistic assessment of the impact of electric vehicles and nonlinear loads on power quality in residential networks. *Int. J. Electron. Power Energy Syst.* **2021**, *129*, 106807. [CrossRef]
10. Nour, M.; Chaves-Ávila, J.P.; Magdy, G.; Sánchez-Miralles, A. Review of positive and negative impacts of electric vehicles charging on electric power systems. *Energies* **2020**, *13*, 4675. [CrossRef]
11. Held, L.; Mueller, F.; Steinle, S.; Barakat, M.; Suriyah, M.R.; Leibfried, T. An optimal power flow algorithm for the simulation of energy storage systems in unbalanced three-phase distribution grids. *Energies* **2021**, *14*, 1623. [CrossRef]
12. Bozalakov, D.; Mnati, M.J.; Laveyne, J.; Desmet, J.; Vandevelde, L. Battery storage integration in voltage unbalance and overvoltage mitigation control strategies and its impact on the power quality. *Energies* **2019**, *12*, 1501. [CrossRef]
13. Dumnic, B.; Popadic, B.; Milicevic, D.; Vukajlovic, N.; Delimar, M. Control strategy for a grid connected converter in active unbalanced distribution systems. *Energies* **2019**, *12*, 1362. [CrossRef]
14. Nejabatkhah, F.; Li, Y.W.; Tian, H. Power quality control of smart hybrid AC/DC microgrids: An overview. *IEEE Access* **2019**, *7*, 52295–52318. [CrossRef]
15. Yu, Y.; Wang, Z.; Wan, X. Optimal current balance control of three-level inverter under grid voltage unbalance: An adaptive dynamic programming approach. *Energies* **2019**, *12*, 2864. [CrossRef]
16. Shigenobu, R.; Nakadomari, A.; Hong, Y.Y.; Mandal, P.; Takahashi, H.; Senjyu, T. Optimization of voltage unbalance compensation by smart inverter. *Energies* **2020**, *13*, 4623. [CrossRef]
17. Moradian, M.; Soltani, J.; Arab-Markadeh, G.R.; Shahinzadeh, H.; Amirat, Y. A new grid-connected constant frequency three-phase induction generator system under unbalanced-voltage conditions. *Electronics* **2021**, *10*, 938. [CrossRef]
18. Jin, Y.; Wang, J.; Liu, Y.; Sai, X.; Ji, Y. Analysis of unbalanced clustered voltage and control strategy of clustered voltage balancing for cascaded H-bridge STATCOM. *J. Mod. Power Syst. Clean Energy* **2019**, *7*, 1697–1708. [CrossRef]
19. Samet, H.; Golshan, M.E.H. A wide nonlinear analysis of reactive power time series related to electric arc furnaces. *Electr. Power Energy Syst.* **2012**, *36*, 127–134. [CrossRef]
20. Yakimov, I.A.; Maklakov, A.S.; Voronin, S.S.; Maklakova, E.A. Results of modeling operation of the high-speed regulator of non-contact secondary voltage of furnace transformer of the high-power arc steel furnace. *Procedia Eng.* **2017**, *206*, 1853–1860. [CrossRef]
21. Lozynskyi, O.Y.; Lozynskyi, A.O.; Paranchuk, Y.S.; Paranchuk, R.Y. Synthesis and analysis of arc furnace electrical mode control system on the basis of three-dimensional phase currents vector distribution. *Electr. Eng. Electromech.* **2019**, *4*, 26–34. [CrossRef]
22. Ali, F.; Arbab, M.N.; Ahmad, G.; Ashraf, M.; Sarim, M. An SVC controller for power quality improvement of a heavily loaded grid. *Mehran Univ. Res. J. Eng. Technol.* **2020**, *39*, 247–256. [CrossRef]
23. Jebaraj, B.S.; Bennet, J.; Kannadasan, R.; Alsharif, M.H.; Kim, M.K.; Aly, A.A.; Ahmed, A.H. Power quality enhancement in electric arc furnace using matrix converter and static var compensator. *Electronics* **2021**, *10*, 1125. [CrossRef]
24. Torabian Esfahani, M.; Vahidi, B. Electric arc furnace power quality improvement by applying a new digital and predicted-based TSC control. *Turk. J. Electr. Eng. Comput. Sci.* **2016**, *24*, 3724–3740. [CrossRef]
25. Lange, A.G.; Redlarski, G. Selection of C-type filters for reactive power compensation and filtration of higher harmonics injected into the transmission system by arc furnaces. *Energies* **2020**, *13*, 2330. [CrossRef]
26. Cernan, M.; Müller, Z.; Josef Tlusty, J.; Valouch, V. An improved SVC control for electric arc furnace voltage flicker mitigation. *Int. J. Electr. Power Energy Syst.* **2021**, *129*, 106831. [CrossRef]

27. Akkaya, S.; Salor, O. Enhanced spectral decomposition method for light flicker evaluation of incandescent lamps caused by electric arc furnaces. *J. Fac. Eng. Archit. Gazi Univ.* **2019**, *34*, 987–1005.
28. Kiyoumarsi, A.; Ataei, M.; Hooshmand, R.; Kolagar, A.D. Electric arc furnace voltage flicker mitigation by applying a predictive method with closed loop control of the TCR/FC compensator. *J. Electr. Eng. Technol.* **2010**, *5*, 116–128. [CrossRef]
29. García-Cerrada, A.; García-González, P.; Collantes, R.; Gómez, T.; Anzola, J. Comparison of thyristor-controlled reactors and voltage-source inverters for compensation of flicker caused by arc furnaces. *IEEE Trans. Power Deliv.* **2000**, *15*, 1223–1231. [CrossRef]
30. Sarma, P.M.; Jayaram Kumar, S.V. Electric arc furnace flicker mitigation in a steel plant using a statcom. *Int. J. Eng. Sci. Innov. Technol.* **2013**, *2*, 227–231.
31. Singh, A.; Singh, R.K.; Singh, A.K. Power Quality Issues of Electric Arc Furnace and their Mitigations—A Review. *Int. J. Adv. Eng. Res. Sci.* **2017**, *4*, 237114. [CrossRef]
32. Łukasik, Z.; Olczykowski, Z. Estimating the impact of arc furnaces on the quality of power in supply systems. *Energies* **2020**, *13*, 1462. [CrossRef]
33. Olczykowski, Z. Modeling of voltage fluctuations generated by arc furnaces. *Appl. Sci.* **2021**, *11*, 3056. [CrossRef]
34. Łukasik, Z.; Olczykowski, Z. Evaluation of flicker of light generated by arc furnaces. *Energies* **2021**, *14*, 3901.
35. Fortescue, C.L. Method of symmetrical coordi-nates applied to the solution of polyphase net-works. *Trans. AIEE* **1918**, *37*, 1027–1140.
36. EN 61000-4-30:2015-05 (EMC)—Part 4-30: Testing and Measurement Techniques—Power Quality Measurement Methods. Available online: https://webstore.iec.ch/preview/info_iec61000-4-30%7Bed3.0.RLV%7Den.pdf (accessed on 15 August 2021).
37. IEC 61000-2-12:2003: Compatibility Levels for Low-Frequency Conducted Disturbances and Signalling in Public Medium-Voltage Power Supply Systems. Available online: https://webstore.iec.ch/publication/4130 (accessed on 15 August 2021).
38. IEC 61000-2-1:1990: Description of the Environment—Electromagnetic Environment for Low-Frequency Conducted Disturbances and Signalling in Public Power Supply Systems. Available online: https://webstore.iec.ch/publication/4127 (accessed on 15 August 2021).
39. ANSI C84.1: American National Standard for Electric Power Systems and Equipment. Available online: https://www.nema.org/Standards/Pages/American-National-Standard-for-Electric-Power-Systems-and-Equipment-Voltage-Ratings.aspx (accessed on 15 August 2021).
40. Engineering Recommendation P29: Planning Limits for Voltage Unbalance in the Unitet Kingdom, The Electricity Council. 1990. Available online: https://www.nienetworks.co.uk/documents/security-planning/er-p29.aspx (accessed on 15 August 2021).
41. GOST 13109–13197: Electric Energy. Electromagnetic Compatibility of Technical Equipment. Power Quality Limits in the Public Power Supply Systems. Available online: http://docs.cntd.ru/document/1200104301 (accessed on 15 August 2021).
42. Kowalski, Z. *Unbalance in Power Systems (Asymetria w układach elektroenergetycznych)*; PWN (Polish Scientific Publishers): Warszawa, Poland, 1987. (In Polish)
43. Olczykowski, Z.; Czyż, J. The Method of Determining the Electrical Parameters, Especially the Resistance and Reactance of the High-Current Path of the Arc Furnace (Sposób Wyznaczania Parametrów Elektrycznych Zwłaszcza Rezystancji i Reaktancji toru Wielkoprądowego Pieca Łukowego). Patent No. 224767, 5 July 2016. (In Polish)
44. International Electrotechnical Commission (IEC). *Test Methods for Direct Arc Furnaces*; IEC standard, Publication 676; Central Office of IEC: Geneve, Switzerland, 1980.
45. Rak, J. Influence of AC ARC Furnace on Parameters of Industrial Medium-Voltage Network. In Proceedings of the 5th International Conference Electrical Power Quality and Utilization, Cracow, Poland, 15–17 September 1999.
46. Ordinance of the Minister of Economy of May 4, 2007 on the Detailed Conditions for the Functioning of the System (Rozporządzenie Ministra Gospodarki z dnia 4 maja 2007 r. w Sprawie Szczegółowych Warunków Funkcjonowania Systemu). Available online: http://prawo.sejm.gov.pl/isap.nsf/DocDetails.xsp?id=WDU20070930623 (accessed on 15 August 2021). (In Polish)
47. PN-EN 50160:2014. *Parameters of the Supply Voltage in the Public Power Networks*; Polish Committee of Standardization; Polish Committee of Standardization: Warsaw, Poland, 2014; 2010p. Available online: https://sklep.pkn.pl/pn-en-50160-2010p.html (accessed on 15 August 2021).